Coherence of Terrestrial Vertebrate Species Richness with External Drivers Across Scales and Taxonomic Groups

Conor P. B. O'Malley[1a], Gareth G. Roberts[1b], Philip D. Mannion[2c], Jan Hackel[3d], Yanghua Wang[1e]

5th September 2022

[1]Department of Earth Science & Engineering, Imperial College London, Royal School of Mines, Prince Consort Road, London SW7 2BP, UK

[2]Department of Earth Sciences, University College London, London WC1E 6BT, UK

[3]Department of Trait Diversity and Function, Royal Botanic Gardens, Kew, London TW9 3AE, UK

[a]*conor.omalley19@imperial.ac.uk*

[b]*gareth.roberts@imperial.ac.uk*

[c]*philipdmannion@gmail.com*

[d]*J.Hackel@kew.org*

[e]*yanghua.wang@imperial.ac.uk*

Corresponding Author: Conor P. B. O'Malley, Royal School of Mines, Prince Consort Road, London SW7 2BP, UK. conor.omalley19@imperial.ac.uk

Data Availability Statement: If the manuscript is accepted, the data supporting the results will be archived on Zenodo: `https://doi.org/10.5281/zenodo.XXXXXX`.

Funding Statement: C.O. was supported by the Leverhulme Trust (Grant: RPG-2019-073, which was awarded to G.R.). P.D.M. was supported by a Royal Society University Research Fellowship (UF160216).

Conflict of Interest Disclosure: The authors declare no conflict of interest.

Authorship Statement: C.O. and G.R. designed the project, developed code, interpreted results and wrote the manuscript with contributions from P.M., Y.W., J.H.; C.O performed the analyses and generated figures.

Acknowledgements: We thank P. Ball, C. Donaldson, F. Richards and A. Whittaker for helpful discussion. Figures were generated using Generic Mapping Tools v6.2.0 (Wessel *et al.*, 2019).

Short Running Title: Coherence of Biodiversity & Environment

Keywords: biodiversity, climate, topography, scale dependence, species richness, spectral analysis

Abstract

Aim: Understanding connections between environment and biodiversity is crucial for conservation, identifying causes of ecosystem stress, and predicting population responses to changing environments. Explaining biodiversity requires an understanding of how species richness and environment co-vary across scales. Here, we identify scales and locations at which biodiversity is generated and correlates with environment.

Location: Full latitudinal range per continent.

Time period: Present-day.

Major taxa studied: Terrestrial vertebrates: all mammals, carnivorans, bats, songbirds, hummingbirds, amphibians.

Methods: We describe the use of wavelet power spectra, cross-power and coherence for identifying scale-dependent trends across Earth's surface. Spectra reveal scale- and location-dependent coherence between species richness and topography (E), mean annual precipitation (Pn), temperature (Tm) and annual temperature range (ΔT).

Results: $> 97\%$ of species richness of taxa studied is generated at large scales, i.e. wavelengths $\gtrsim 10^3$ km, with 30–69% generated at scales $\gtrsim 10^4$ km. At these scales, richness tends to be highly coherent and anti-correlated with E and ΔT, and positively correlated with Pn and Tm. Coherence between carnivoran richness and ΔT is low across scales, implying insensitivity to seasonal temperature variations. Conversely, amphibian richness is strongly anti-correlated with ΔT at large scales. At scales $\lesssim 10^3$ km, examined taxa, except carnivorans, show highest richness within the tropics. Terrestrial plateaux exhibit high coherence between carnivorans and E at scales $\sim 10^3$ km, consistent with contribution of large-scale tectonic processes to biodiversity. Results are similar across different continents and for global latitudinal averages. Spectral admittance permits derivation of rules-of-thumb relating long-wavelength environmental and species richness trends.

Main conclusions: Sensitivities of mammal, bird and amphibian populations to environment are highly scale-dependent. At large scales, carnivoran richness is largely independent of temperature and precipitation, whereas amphibian richness correlates strongly with precipitation and temperature, and anti-correlated with temperature range. These results pave the way for spectral-based calibration of models that predict biodiversity response to climate change scenarios.

1 Introduction

Biological diversity is critical to many basic human needs, including health, food, water and shelter. It also plays an important role in moderating physical and chemical processes in natural environments

(Balmford & Bond, 2005; Barrett *et al.*, 2011; Corenblit *et al.*, 2011; Fei *et al.*, 2014; Mori *et al.*, 2022). Quantifying links between environment and biodiversity is crucial for understanding the response of ecosystems to climatic and physiographic change, and for conservation efforts (Araújo & Rahbek, 2006; Hampe & Petit, 2005; Norris *et al.*, 2013; Yasuhara *et al.*, 2020a). Many extrinsic processes postulated to control biodiversity (e.g. climate) are rapidly changing; therefore quantifying the strength of relationships between them is a pressing concern (Nogués-Bravo *et al.*, 2018).

Environmental variables and species richness exhibit variance in space across a range of scales (e.g. Belmaker & Jetz, 2011; Buckley *et al.*, 2012; Keil & Chase, 2019). However, it is unclear whether coherence between variables is uniform across all scales Storch *et al.* (2007). In this study we test the following five hypotheses. First, species richness is highly coherent with environmental variables across all scales. That would imply a direct forcing of richness by external drivers regardless of scale. It would give a basis for using theory developed to predict species richness at one scale (e.g. field sites) to predict richness at all scales. Secondly, species richness is most coherent with external variability at small scales, i.e. local changes in environment determine where species richness prospers. Thirdly, species richness is most coherent with changes in environment at large scales, i.e. global scale variability (e.g. large-scale climate change). Fourthly, the coherence of species richness with external variables depends on taxon. In other words, taxa have unique responses to environment variables. Finally, species richness does not directly depend on environment (i.e. coherence between species richness and environmental variables is low). Instead, species richness depends upon other factors, namely biotic interactions (prey-predator, competition), and/or historical contingencies.

Here, we test the five hypotheses by quantifying coherence between species richness of continental vertebrate taxa and elevation, precipitation, temperature, and annual temperature range, which are postulated to drive biodiversity (e.g. Antonelli *et al.*, 2018; Rahbek & Graves, 2001). As a starting point, we focus on mapping coherence between contemporary biotic and environmental signals as a function of scale and location, using wavelet spectral analyses. Many existing approaches, e.g. spatial regression analyses, are unsuited to testing such hypotheses because of the challenges associated with disentangling scale and location from biotic and environmental data to identify correlations. Instead, here, we use wavelet spectral analyses, which inherently disentangle scale-dependent effects, and identify strength of correlation between variables at individual scales. Such analyses have been used to identify scale-dependence of temporal biotic series, to filter spatial series and identify outliers, and to investigate biodiversity on local ($\lesssim$ 500 km) scales (Carl *et al.*, 2008, 2016; Dormann *et al.*, 2007; Keitt, 2007; Ma & Zhang, 2015; Roberts & Mannion, 2019). We acknowledge that other processes, including species-species interactions, are also important for determining species richness (e.g. Chaudhary *et al.*, 2021; Yasuhara *et al.*, 2020b; Yasuhara & Deutsch, 2022). As such, we also present a preliminary

assessment of the coherence between species richness of different taxa, in Supporting Information. We return to discuss the results of these tests in the context of the five hypotheses described above, in the concluding section of this manuscript.

Identifying links between biodiversity and environment has recently become significantly more tractable for three reasons. First, global patterns of species richness have been estimated with unprecedented detail, from horizontal scales as broad as continents, to those as fine as $\sim$ 10 km in wavelength (e.g. Jenkins & Joppa, 2009; Jenkins *et al.*, 2013, 2020; Kass *et al.*, 2022; Marsh *et al.*, 2022). Second, values and variance of many environmental variables postulated to be responsible for determining distributions of species are now available globally at even higher resolution (e.g. Karger *et al.*, 2017). Finally, wavelet spectral methods, which can identify the locations and scales at which signals (e.g. spatial series of taxa) are generated, as well as coherence and phase differences (offsets) between series such as species richness, topography and climate, are now established (see Materials and Methods; Grinsted *et al.*, 2004; Torrence & Compo, 1998). Such analyses are key to understanding how the changing global climate will affect the distribution of biodiversity across Earth.

2 Materials and Methods

2.1 Species Richness Data

Species richness is here defined as number of species of a given taxon within a 10×10 km square. We use the grids compiled by Jenkins *et al.* (2013), which were generated by combining maps of species distributions, and counting the number of overlapping polygons in a given cell. For birds, the species richness data were calculated from breeding ranges compiled by BirdLife International NatureServe (2011). For amphibians and mammals, the data were based on expert range maps generated by the International Union for Conservation of Nature (2021).

Figure 1a–f shows species richness per 10×10 km cell for all mammals (Mammalia), carnivorans (Carnivora), bats (Chiroptera), songbirds (Passeriformes), hummingbirds (Trochilidae), and amphibians (Amphibia). In Supporting Information Figures 1–2, we show species richness and associated analyses for other evaluated taxonomic groups (including Cetartiodactyla, Eulipotyphla, primates, marsupials, rodents, parrots, and frogs). The taxa which we focus on in the main text of this study have the greatest latitudinal coverage and are well-mapped, and they also cover a range of modes of life. The data shown in Figure 1 reinforce well-known large-scale observations, e.g. the latitudinal diversity gradient, but also contain evidence of significant complexity across scales of interest, here wavelengths

between 10–10^4 km (e.g. Hillebrand, 2004; Willig *et al.*, 2003). We examine species richness trends in this study, since it is a straightforward measure of diversity, and has been determined for a wide range of taxa from fine scales up to near global scales. Here, we focus on terrestrial vertebrate taxa since terrestrial surface environmental conditions are well-mapped, as is terrestrial vertebrate biodiversity. Similar analysis is possible for marine taxa, invertebrates, plants etc., and for metrics other than species richness, for example range sizes and trophic interactions.

Species richness varies as a function of the spatial range characteristics of a study, particularly "grain", i.e. piece-wise horizontal resolution within a study (Gaston, 2000; Palmer & White, 1994; Willig *et al.*, 2003). By using a constant grain (i.e. "focus" or grid spacing) of 10 km, challenges associated with comparing results generated using different grains are avoided (Willig *et al.*, 2003). Here, scale-dependent trends are calculated as a function of "extent", i.e. total width of study region, rather than "grain", i.e. width of each plot/grid cell within the study region *sensu* Palmer & White (1994). Hurlbert & Jetz (2007) indicated that range map data might only be valid at wavelengths > 100 km. In this study, we evaluate how short-wavelength uncertainties in species richness contribute to uncertainties in calculated wavelet spectra by adding theoretical noise to transects before they are transformed into the spectral domain (Supporting Information Figure 3; panels a–c show results of adding white noise which has wavelengths between 10–100 km). Latitudinal transects through terrestrial vertebrate richness and environmental data are shown in Figure 2. We show data from the Americas, where transects can be generated that encompass almost all of Earth's latitudinal range (Figures 1 & 2: A—A′). Transects through data for Australia (B—B′), Africa (C—C′), Eurasia (D—D′) and global averages are shown in Supporting Information Figures 4–7.

2.2 Environmental Variable Data

Figures 1g–j and 2m, o, q and s show examples of maps and cross sections through elevation and climatic data which we use, from the ETOPO1 and CHELSA datasets, respectively (Amante & Eakins, 2009; Karger *et al.*, 2017).

The global elevation grid ETOPO1 has a horizontal resolution of 1 arc-minute (Figure 1g; Amante & Eakins, 2009). It is primarily generated from $\sim$ 30 m resolution Shuttle Radar Topography Mission (SRTM30) data and includes interpolated coastlines and satellite altimetry (Jarvis *et al.*, 2008). Amante & Eakins (2009) suggested a mean vertical error of $\sim$ 10 metres for ETOPO1. We down-sampled the data to a horizontal resolution of 10 km using Generic Mapping Tools to match resolution of species richness grids (Wessel *et al.*, 2019).

Annual mean values for climatic data, from 1981–2010, were extracted from the Climatologies at High Resolution for the Earth's Land Surface Areas (CHELSA) dataset (Karger *et al.*, 2017). CHELSA was generated by applying corrections to the ERA-Interim climatic reanalysis and has a horizontal resolution of up to 30 arc-seconds (Dee *et al.*, 2011). Temperature data were corrected for elevation above sea level and precipitation rates were corrected using wind direction, valley exposition and boundary layers. Precipitation rate is weakly dependent on elevation. These values were successfully benchmarked against alternative climatology data and models: WorldClim, TRMM , GPCC and GHCN (Hijmans *et al.*, 2005; Goddard Earth Sciences Data and Information Services Center, 2017; Lawrimore *et al.*, 2011; Schneider *et al.*, 2014). The data were down-sampled to 10 km prior to spectral analyses.

2.3 Continuous Wavelet Transform

Spatial series, x_n, of species richness or environmental variables were transformed into distance-wavenumber space using continuous wavelet transforms (for practical guide, see Torrence & Compo, 1998). The transform convolves uniformly sampled spatial series with a mother wavelet, ψ. The Morlet wavelet with dimensionless frequency $\omega_\circ = 6$ is used in this study, although other mother wavelets are investigated in Supporting Information Figure 8. Use of different mother wavelets (Morlet, order $\omega_\circ = 4$, 8; Paul, order $m = 2$, 4, 6; derivative of Gaussian, order $m = 2$, 4, 6) does not significantly change patterns of mapped power, and distance-averaged power shows similar trends to the results presented here. The mother wavelet is scaled and translated along spatial series by n' to reveal variations in amplitude as a function of scale, s, and position, x_n. Sampling interval $\delta t = 10$ km, $n = 0, 1 \ldots N-1$, where N is number of measurements. The wavelet transformation is

$$W_n(s) = \sum_{n'=0}^{N-1} x_n \psi^* \left[\frac{(n'-n)\delta t}{s} \right], \tag{1}$$

where $*$ denotes the complex conjugate. We use the mlpy Python module to transform the spatial series (Albanese *et al.*, 2012), which is based on the methods summarized by Torrence & Compo (1998). Scales were calculated using the approach described in Torrence & Compo (1998), such that $s_j = s_\circ 2^{j\delta_j}$, where $j = 0, 1, \ldots J$. The smallest scale, $s_\circ = 2\delta t$. A minimum grid spacing of 10 km therefore yields a minimum scale for wavelet spectral analysis of ~ 20 km (Torrence & Compo, 1998). In the example shown in Figure 2, $N = 1598$, $\delta_j = 0.1$ and $J = 96$, which yields a total of 97 scales that range from $\sim$ 20 to $\sim$ 15,521 km. Spatial series were mirrored across the x (distance) and y (dependent variable) axes to reduce edge effects (Roberts *et al.*, 2019). Inverse transforms were reconstructed for each signal to quantify fidelity of transformed series (see Torrence & Compo, 1998). Median difference between input signals and inverse transforms were always $\leq 0.9\%$. Signals can be filtered by calculating inverse transforms at specific wavelengths. For example, Figure 2a, c, e, g, i and

k show inverse transforms of species richness spectra at scales $> 10^3$ km. Depending on taxonomic group, these filtered signals fit the input species richness trends with mean differences of 4.4–25% (see Figure 2 caption for mean raw differences in terms of species per pixel, spx). The same filtering process, but including wavelengths $> 10^2$ km, yields mean differences of only 0.7–4.7%. The distance-averaged power spectrum, which yields similar results to Fourier transformation, is given by

$$\phi(s) = \frac{1}{N} \sum_{x=0}^{N} |W_n(s)|^2. \tag{2}$$

In Figure 2, we plot rectified distance-averaged power $\phi_r = \phi(s)s^{-1}$ after Liu *et al.* (2007). We calculate distance-averaged power within and outside of the tropics, but note that in those calculations, power was normalized by the proportion of the transect within/outside of the tropics respectively. Therefore there is no bias in distance-averaged power if the transect has a greater distance within/outside of tropical latitudes. A guide to scale-dependence and self-similarity of spatial series is the color of spectral noise that they possess. For example, red (Brownian) noise occurs when $\phi \propto k^{-2}$, where k is wavenumber or spatial frequency, proportional to 1/wavelength, indicating self-similarity. Pink noise occurs when $\phi \propto k^{-1}$, and white noise indicates that power is equal across all scales, $\phi \propto 1$. Best-fitting spectral slopes for all variables and transects were identified using simple one- and two-slope models after Roberts *et al.* (2019); see Supporting Information Figures 9–18.

2.4 Cross Wavelet Power & Wavelet Coherence

Cross wavelet power is calculated to identify signals in separate spatial series (e.g. amphibian richness and precipitation) that have large amplitudes located at the same position in distance-wavenumber space. To facilitate comparison, signals are normalized to zero mean and unit variance prior to transformation. The normalized signals X and Y, are transformed to yield W^X and W^Y. Cross wavelet power W^{XY} is calculated such that

$$W^{XY} = W^X W^{Y^*}, \tag{3}$$

where $*$ denotes complex conjugation. Wavelet coherence, R_n^2, is calculated to identify parts of signals that are coherent, but not necessarily of common high amplitude, such that

$$R_n^2(s) = \frac{|S\{s^{-1} W_n^{XY}(s)\}|^2}{S\{s^{-1}|W_n^X(s)|^2\} \cdot S\{s^{-1}|W_n^Y(s)|^2\}}, \tag{4}$$

where s, n and $W_n(s)$ are as in Equation 1. S is an operator that smooths along distance and scale (Grinsted *et al.*, 2004).

Signals with certain spectral distributions (e.g. red noise) can, by chance, correlate without true

interdependence. Therefore, it is important to calculate the coherence between each pair of signals, and not simply their cross wavelet power. Torrence & Compo (1998), Grinsted *et al.* (2004) and others have shown that coherence between signals above (assumed) background noise (i.e. spectral distributions) can be estimated by first calculating the coherence between large numbers of surrogate datasets with the same autoregressive (AR) coefficients as the original data set. In this study, the minimum bound for statistically significant coherence (above assumed background noise) per scale, for each transect, was calculated from cross wavelet power spectral analysis of 300 random signals. Guided by the spectral content of actual biotic and environmental signals, we assumed that each theoretical random signal has a red noise distribution, which was generated using the same autocorrelation coefficient as the actual input signals. The surrogates also have the same length and number of measurements, N, as the actual signals. The 90% significance limit for coherence, which was used to mask Figure 3, depends only on scale and not position, and was calculated using Monte Carlo methods with the PyCWT Python module (Grinsted *et al.*, 2004; Krieger *et al.*, 2020).

The local phase difference (angular offset, $0 \leq a \leq 2\pi$) of two signals is given by the complex argument of their cross wavelet transform, $\arg\left(W^{XY}\right)$ (Grinsted *et al.*, 2004). Figure 3 indicates phase difference as arrows measured from horizontal: in-phase, $a = 0$, $\triangleright$; anti-phase, $a = \pi$, $\triangleleft$. A working example for species richness and elevation, including continuous wavelet transformation, cross wavelet power and wavelet coherence calculations, can be found at `https://doi.org/10.5281/zenodo.XXXXXX`.

3 Results and Discussion

3.1 Wavelet Transformation of Richness and Environmental Variables

Spectral analyses of vertebrate species richness and environmental variables are shown in Figures 2 and 3. Figure 2 shows that highest spectral power, ϕ ($\propto z^2$, where z is signal amplitude), is concentrated at largest scales for all taxa and environmental variables studied. Dependent on taxonomic group, from 96% to almost 100% of power resides at wavelengths $> 10^3$ km. 30–69% of power resides at wavelengths $\gtrsim 10^4$ km. These results reinforce the notion that species richness is dominated by long wavelength, latitudinal, variability.

Species richness tends to have a pink noise spectrum (see Supporting Information Figures 9–18). Thereby, shorter wavelength features in species richness signals tend to have the lowest amplitudes and comprise relatively little (few %) of species richness signal at a particular location. Mammals and bats are better characterized by red noise at long wavelengths. This result implies self-similarity

across scales, and that signal amplitudes decrease even more rapidly with decreasing wavelength than for other taxa. At wavelengths $\gtrsim 10^3$ km, species richness power for amphibians is best characterized as blue noise, i.e. $\phi \propto k^1$. This trend is not observed along the entire transect, but indicates that short wavelength features can be increasingly important contributors to amphibian richness (see Figure 2f). A single spectral slope akin to pink noise can adequately fit the amphibian richness spectrum (see e.g. Supporting Information Figure 9f).

We address concerns regarding the accuracy of range maps in two ways. First, we show the results of inverse wavelet transforms at scales > 1000 km alongside the results for transformation of the full frequency content of the available data. Secondly, we explore the impact of inserting distributions of theoretical, hitherto unknown, species in a suite of increasing severe tests for our results and conclusions. White noise was added to the amphibian transect in a systematic set of tests. These tests examined changes in calculated spectra when noise with maximum amplitudes of 10%, 50% and 100% of the standard deviation of the original signal's amplitude (in this case = 24 species per pixel) was added to the transect prior to transformation. These tests included adding noise at wavelengths $\lesssim 100$, $\lesssim 1000$ and $\lesssim 10,000$ km (Supporting Information Figure 3). As expected, these tests indicated that spectral power is least likely to be well constrained at short wavelengths. Nonetheless, these tests indicate that even high amplitude uniformly distributed noise does not significantly change the overall spectral characteristics of terrestrial species richness. Finally, we note that that Hurlbert & Jetz (2007) suggest that species richness values estimated from range maps are likely to be overestimates at short length scales compared to richness estimated from atlas data (e.g. their Figure 5). That result indicates that range maps are more likely to generate higher power at short wavelengths than maps derived from atlas data. Therefore, spectra derived from atlas data are likely to be even redder than those obtained from range maps. In other words, our conclusion that species richness is dominated by long wavelength structure is expected to be insensitive to the choice of range or atlas data. In fact, atlas data is likely to more strongly emphasize the importance of long wavelength variability for determining species richness. We suggest that these observations and results indicate that range maps are useful for our purposes.

Although almost no power is concentrated below wavelengths of $\sim$ 100 km for any of the taxa examined here, there are regions of some wavelet transforms which show increased power in the range $\sim$ 300–1000 km. This deviation, away from a broadly monotonic decrease in power towards shorter wavelengths, is driven principally by species richness within tropical latitudes, and is especially prominent for songbirds, hummingbirds and amphibians (Figure 2h, j, l). Supporting Information Figure 19a–f shows that at wavelengths $\gtrsim 1000$ km, there is no notable difference between power in species richness within or outside the tropics, across the Americas. However, at wavelengths $\lesssim 1000$ km, there

is significantly greater power for regions within the tropics. This trend arises because power spectral slopes remain close to -2 at shorter wavelengths outside of the tropics (i.e. red noise; Supporting Information Figure 19), before increasing to be closer to -1 (i.e. pink noise). We suggest that these results are consistent with the concept that topography in tropical regions can generate higher species richness towards the equator via the increased effectiveness of altitudinal variation in habitat at isolating species either physically or physiologically (i.e. by being associated with variation in other environmental variables such as temperature; Ghalambor *et al.*, 2006; Janzen, 1967). We find the effect has a greatest impact on species richness power of hummingbirds and amphibians; the impact on bats and songbirds richness appears to be more modest. Tropical increases in species richness of carnivorans, and mammals more generally, are much more subdued (Supporting Information Figure 19).

Elevational transects exhibit red and pink noise spectral characteristics at wavelengths $\gtrsim 10^3$ km and $\lesssim 10^3$ km, respectively, which we note is similar to distance-averaged power from wavelet transforms of longitudinal river profiles and other topographic transects (Supporting Information Figures 9g, 9q, 10g, 10q; Roberts *et al.*, 2019; Wapenhans *et al.*, 2021). Precipitation rate, temperature and annual temperature range can also be characterized as red and pink noise (Supporting Information Figures 9h–j, r–t & 10h–j, r–t). Similar results are obtained for latitudinal transects through Africa, Eurasia and Australia, as well as across global, latitudinally-averaged sections (see Supporting Information Figures 11–23).

3.2 Coherence between Richness and Environment

Visual inspection of Figure 2 indicates that there is strong, location- and scale-dependent, similarity between the wavelet transforms of transects through species richness and environmental variables. To quantify the strength of these relationships we calculate cross wavelet power, which identifies co-located high amplitudes in the location-scale domain, and wavelet coherence (see Materials and Methods). Figure 3 shows results for carnivorans (which are similar to those for mammals generally), and amphibians (which are similar to those for bats, songbirds and hummingbirds). See Supporting Information Figure 1–2 for analyses of those other taxa. Figure 3a shows cross wavelet power between species richness of carnivorans along transect A—A′ and elevation. Almost no short-wavelength ($< 10^3$ km) features are coherent above a 90% confidence limit. These short wavelength regions contain almost no cross wavelet power; 94% of all cross wavelet power is in the region of high coherence colored on Figure 3a, which accounts for 30% of the location-scale domain. 79% of the area of the cross wavelet spectrum that is significantly coherent resides at wavelengths $\gtrsim 10^3$ km. Distance-averaged cross wavelet power for all parts of the power spectrum, not just those parts which are coherent above the 90% significance

threshold, is shown to the right of each panel, on a logarithmic scale. Full, unmasked, plots of cross wavelet power are shown in Supporting Information Figure 24. Masked and unmasked cross power plots for other transects and global latitudinal averages are shown in Supporting Information Figures 25–32. Distance-averaged cross wavelet power between all taxa and environmental variables studied is shown in Supporting Information Figures 19–23, panels g–ad.

Cross wavelet power between amphibians and elevation is also highest at long wavelengths, although overall there is a smaller proportion of the two signals that is coherent: 78% of the plot region is masked in Figure 3e (gray regions). Only a small part of the cross wavelet transform for amphibians and elevation is coherent below wavelengths of ~ 5000 km, and that part lies near the centre of the transect, i.e. within the tropics. Distance-averaged power outside the tropics, plotted to the right of Figure 3e as a gray curve, is an order of magnitude lower than within the tropics, especially at wavelengths $\lesssim 3000$ km. This observation is in contrast to cross power between species richness of carnivorans and elevation, where there is almost no difference between the results within and outside of the tropics, across all scales. These results may indicate that carnivorans are less affected by "mountain passes" (*sensu* Janzen, 1967) in the tropics, compared with amphibians (cf. Antonelli *et al.*, 2018; Eronen *et al.*, 2015; Rahbek *et al.*, 2019; Rolland *et al.*, 2015). At wavelengths $\sim 10^3$ km, carnivoran species richness is most coherent with elevation and mean annual temperature atop terrestrial plateaux (e.g. Rocky-Mountains-Colorado Plateau and Altiplano, between $4000 - 7000$ km and $13,000 - 14,000$ km distance along transect A—A′, respectively; Figures 1–3). An obvious interpretation is the local importance of tectonics for determining biodiversity (Antonelli *et al.*, 2018).

Statistically significant (above background red noise), coherent cross wavelet power between carnivoran species richness, mean annual precipitation rate, temperature and annual temperature range is shown in Figure 3b–d. Results for amphibians are shown in panels f–h. Cross power between amphibian species richness and precipitation rate, temperature, and temperature range tends to be higher within the tropics compared to outside the tropics at wavelengths $\lesssim 3000$ km (cf. grey, blue, black lines in Figure 3). Those differences are absent or reduced for carnivorans. Furthermore, a smaller area of the power spectra of these three climatic variables is significantly coherent with carnivoran richness, compared to amphibian richness (cf. extent of gray masks in Figure 3). One likely interpretation of these results is that carnivorans are less sensitive to changes in those variables than amphibians (e.g. Rolland *et al.*, 2018). Calculated phase indicates long-wavelength anticorrelation between elevation and species richness for both carnivorans and amphibians (left-pointing arrows in Figure 3a and e; phase angle, $a = \pi$; see Materials and Methods). Highly coherent long-wavelength anticorrelation between amphibian species richness and annual temperature range is also observed across the entire transect. Highly coherent, long-wavelength cross power between precipitation rate or temperature,

and species richness of both carnivorans and amphibians, is in phase, i.e. there is positive correlation at these scales. This result is in agreement with the idea that faster diversification rates contribute to heightened species richness, since it suggests that both taxonomic groups benefit from increased energy and higher productivity associated with greater availability of heat and water (cf. Allen *et al.*, 2006).

3.3 Global and Local Species Richness and Environment

These results for the Americas can be compared to transects from Australia, Eurasia and Africa. For Australia, similar trends in power spectral slopes, distance-averaged power and cross wavelet power are observed (Figure 1: B—B′; Supporting Information Figures 4, 11–12, 20, 25–26). However, for Australia there is almost no difference in power or cross power between tropical regions and regions outside the tropics. We note, however, that the Australian transect does not include the entirety of the tropics; it only spans latidudes between 11.2°S–37.6°S. Signals are mostly coherent at wavelengths $\gtrsim 10^3$ km, and the same pattern of correlation/anticorrelation is observed with climatic variables as that recovered for the Americas (Supporting Information Figures 25–26). In Africa, songbirds and amphibians have greater species richness power within the tropics but the differences outside of the tropics are not as stark as for the Americas (Figure 1: C—C′; Supporting Information Figure 21a–f). This result may reflect differences in Cenozoic paleoclimatic history between Africa and the Americas (Hagen *et al.*, 2021). The greatest difference between cross power within and outside the tropics is for precipitation rate, suggesting that water availability is a more important control species richness for all African taxa studied here. Wavelet coherence indicates that, across Africa, carnivoran species richness does not correlate with environmental variables, whereas species richness of amphibians is strongly positively correlated with precipitation rate at long wavelengths, in agreement with the findings of Buckley & Jetz (2007). Anticorrelation is observed between amphibian species richness and temperature across Africa. Results for Eurasia are dominated by the presence of the Tibetan Plateau, and the low proportion of the transect within tropical latitudes (Figure 1: D—D′; Supporting Information Figures 6, 15–16, 22, 29–30). Similar trends to the Americas are observed, albeit with generally lower cross power and coherence.

Mean terrestrial values of each variable across all latitudes globally were transformed into the location-scale domain. Distance-averaged wavelet power spectra of the resulting transects have spectral slopes between -2 and -1 (red to pink noise), reflecting the importance of long-wavelength trends. Species richness power for all taxa, except Mammalia and Carnivora, is at least an order of magnitude lower outside of tropical latitudes, at wavelengths $\lesssim 3000$ km, consistent with results obtained from

transforming the American transect (Figures 2 and 3). This result suggests that the increase in species richness power at short wavelengths may be a global phenomenon, reflecting sensitivity of tropical species to local climatic effects.

Figure 4a–f shows a summary of results for the transect across the Americas, A—A′. Panels a and b show inverse wavelet transforms generated using only the the longest 20% of scales (wavelengths $\gtrsim$ 3750 km; approximately one quarter of the length of the transect), for amphibian and carnivoran species richness respectively. Those taxa have significantly different modes of life and their wavelet power, cross power and coherence with environment exhibit the greatest differences of any taxa studied. These low-pass filtered series account for $\sim$ 41 and $\sim$ 11% of species richness in terms of mean difference to input, respectively. Figure 4c–f shows inverse wavelet transforms of environmental series filtered in the same way. Coherence, R_n^2, between the filtered series and amphibian (green) and carnivoran (purple) species richness trends is annotated on each panel. These results for the Americas are consistent with global averages, although coherence is generally lower for global results since regions of common power may not be generated at the same longitudes (see Figure 4g–l).

3.4 Transfer Functions Between Environment and Species Richness

It is useful to derive 'rules-of-thumb' to estimate species richness from environmental variables. This study indicates that such conversion schemes (transfer functions) are likely to be particularly useful at large scales where most species richness appears to be determined, and where coherence with environmental variables is highest. In the scale-distance domain, after wavelet transformation (see Methods and Materials), species richness W of any given taxon X can be expressed:

$$W^X(x,s) = Z^{X\epsilon}(x,s) \cdot \epsilon(x,s) + \eta, \tag{5}$$

where x is distance, s is scale, and η is noise or contributions from variables that have not been considered. $Z^{X\epsilon}$ refers to the admittance (transfer function) between a set of environmental variables ϵ, and richness in the scale-distance domain, W^X. For any individual variable Y within ϵ, the admittance between W^X and W^Y can be expressed:

$$Z^{XY}(x,s) = \frac{W^X W^{Y*}}{W^Y W^{Y*}}, \tag{6}$$

where * denotes complex conjugate. Thereby, a species richness signal X can be estimated from calibrated admittance Z^{XY}, by convolving the inverse transform of Z^{XY} with Y (see Methods and Materials; Torrence & Compo, 1998).

Table 1 and Figure 4 show estimates of admittance between environmental variables and amphibian and carnivoran richness series for the largest 25% of scales (wavelengths $\geq$ 3756 km). The mean of the transfer function between mean annual precipitation (i.e. W^Y) and amphibian richness (W^X) in the Americas, for example, is $12.7^{+5.3}_{-3.2}$ spx/m. These scales account for $\gtrsim 60\%$ of observed amphibian species richness. Stated uncertainties are distances to 1st and 3rd quartiles of admittance values, across all (x, s) space for $s \geq 3756$ km. Calculated admittance is most likely to be a reliable rule of thumb for converting environmental variable values into species richness when coherence is high. In Table 1, bold values indicate values where coherence is > 0.5. For example, consider the mean large-scale coherence between amphibian richness and precipitation, which is 0.76 ± 0.2. This result, coupled with the associated high positive admittance value, is suggestive of amphibian richness dependence on large-scale precipitation patterns. Compare that result to the relatively low mean large-scale coherence between American carnivoran richness and annual temperature range, which is only 0.22 ± 0.2, reflecting their likely independence. A comparison with results generated using global mean species richness and environmental variables indicates that these rules are generally applicable (see Table 1 & Figure 4). Such simple rules-of-thumb appear to provide a means to predict species richness from external variables at large ($\gtrsim$ 1000 km) scales.

Table 1: Rules of thumb to convert values of environmental variables into species richness. E = elevation, Pn = mean annual precipitation, Tm = mean annual temperature, ΔT = annual temperature range (see Figures 1–2). Z = admittance (transfer function) between environmental variables and species richness at large scales ($>$ 3756 km); subscripts AA & MA indicate American amphibians & mammals; subscripts AG & MG indicate global amphibians & mammals; units are spx/km, spx/m or spx/°C, where spx = species per pixel. R^2_n = coherence between environmental variable and species; bold = admittance and coherence values for species-variable relationships with mean $R^2_n > 0.5$

Variable	Z_{AA}	R^2_n	Z_{MA}	R^2_n	Z_{AG}	R^2_n	Z_{MG}	R^2_n
E, km	$\mathbf{-7.6^{+3.0}_{-2.5}}$	$\mathbf{0.52 \pm 0.3}$	$\mathbf{-1.7^{+0.6}_{-1.1}}$	$\mathbf{0.62 \pm 0.2}$	$2.5^{+15.5}_{-17.7}$	0.14 ± 0.1	$-1.3^{+5.5}_{-6.4}$	0.13 ± 0.1
Pn, m	$\mathbf{12.7^{+5.3}_{-3.2}}$	$\mathbf{0.76 \pm 0.2}$	$\mathbf{2.5^{+2.0}_{-0.9}}$	$\mathbf{0.51 \pm 0.2}$	$14.0^{+10.1}_{-7.5}$	0.41 ± 0.2	$1.8^{+2.2}_{-2.5}$	0.21 ± 0.2
Tm, °C	$0.9^{+0.8}_{-1.0}$	0.31 ± 0.2	$0.2^{+0.2}_{-0.3}$	0.28 ± 0.2	$-0.4^{+3.0}_{-2.3}$	0.46 ± 0.2	$\mathbf{-0.3^{+0.7}_{-0.5}}$	$\mathbf{0.55 \pm 0.3}$
ΔT, °C	$-0.4^{+0.9}_{-0.5}$	0.26 ± 0.3	$-0.1^{+0.3}_{-0.1}$	0.22 ± 0.2	$-0.7^{+0.7}_{-0.7}$	0.28 ± 0.2	$0.0^{+0.1}_{-0.2}$	0.29 ± 0.2

3.5 Drivers of Species Richness

In the introduction of this paper we described five hypotheses to test. First, we hypothesized that species richness is highly coherent with environmental variables across all scales. Given the spectral analyses we present, which indicate that most species richness does not have statistically significant coherence with environmental variables at wavelengths $\lesssim$ 1000 km at most latitudes, this hypothesis can be rejected. Our second hypothesis—species richness is most coherent with external variability at small

scales—is also thus rejected. Our third hypothesis—species richness is most coherent with changes in environment at large scales—was found to be reasonable. Generally, our results indicate that species richness is most coherent with environment at wavelengths $\gtrsim 10^3$ km, where highest species richness power also resides. Our fourth hypothesis—that coherence of species richness with external variables depends on taxonomic group—was also found to be reasonable. For example, amphibian richness is found to be highly coherent with temperature range at scales > 5000 km, whereas carnivoran richness has very low coherence at these scales (cf. Figure 3d and 3h). Furthermore, amphibian richness seems to be more coherent with precipitation and temperature within the tropics, while carnivoran richness is not. Our fifth and final hypothesis—that species richness does not directly depend on environment, instead, species richness depends upon biotic interactions—requires modification. Species richness was found to have both high and low coherence with environmental variables, depending on location, scale and the environmental variable being considered. We have shown that wavelet transformation provides a means to identify coherence in the space-frequency domains. Our preliminary assessment of species-species interactions indicates that their coherence is also scale- and location-dependent (Supporting Information Figure 2). However, we note that calculated coherence and cross power between species tends to be lower than that between species and environmental variables. We note that historical effects, i.e. speciation/extinction rates over geologic time, are not identified within this study, solely modern correlations between variables, although long-term speciation/extinction rates may themselves depend on environment (e.g. Skeels *et al.*, 2022). Nonetheless, we tentatively suggest that these results indicate that environment is more important in determining species richness than species-species interactions.

3.6 Implications for Macroecological Biodiversity Patterns

A principal result of this study is that terrestrial species richness tends to be most coherent with topography, precipitation and temperature at long wavelengths ($> 10^3$ km). These results indicate that large-scale variation in tectonic and climatic processes play a governing role in generating the latitudinal diversity gradient (Field *et al.*, 2009). However, our results also indicate that the distribution of taxa, and their coherence and phase with environmental variables, is highly location- and scale-dependent. For example, whereas carnivorans and amphibians are in phase and coherent with mean annual precipitation and temperature at wavelengths $> 10^4$ km, that is not true at smaller scales (i.e. shorter wavelengths). Significant deviations from the latitudinal diversity gradient indicate that external variables such as elevation, climatic patterns and tectonic history, play important roles in determining biodiversity at specific locations and scales (e.g. Archibald *et al.*, 2010, 2013; Hagen *et al.*, 2021; Jones *et al.*, 2022; Mannion *et al.*, 2014; Saupe, 2021; Song *et al.*, 2020; Yasuhara *et al.*, 2017).

Spectral analyses highlight the importance of the tropics for biodiversity, in particular for amphibians, for which local changes in elevation and mean annual temperature (but not annual temperature range) are highly coherent with species richness. These results are consistent with the idea that increased resource availability in the tropics may generate higher primary productivity, supporting a greater number of individuals within a given area (i.e. higher carrying capacity), and therefore a greater number of different species (e.g. Fritz *et al.*, 2016; Gillman *et al.*, 2015; Hawkins *et al.*, 2003; Kessler *et al.*, 2014). Our results support the suggestion that elevated topography at the tropics is more likely to result in increased species diversity when compared to higher latitudes (Ghalambor *et al.*, 2006; Janzen, 1967; Polato *et al.*, 2018). However, this trend is not uniformly observed across taxa and for all continents. Species richness of carnivorans, for example, has no significant coherence with elevation or temperature range in the tropics, which suggests that this group is largely unaffected by the challenges posed by tropical mountain ranges. This might reflect the group's relatively unusual biogeographical history and seemingly high dispersal ability, with carnivorans originating at high latitudes and dispersing into the tropics, with net diversification rates comparable in tropical and temperate regions (Rolland *et al.*, 2015). Power spectral slopes for such taxa are steeper (more negative) at shorter wavelengths, whereas more environmentally-sensitive taxa, such as hummingbirds and amphibians, have shallower spectral slopes at longer wavelengths within tropical latitudes.

Cross wavelet power and coherence indicate that species richness is decoupled from short wavelength ($\lesssim 10^3$ km) changes in elevation, temperature, annual temperature range and precipitation at nearly all locations, except for certain taxa within the tropics. Locally, uplifted topography can be highly coherent with species richness. Trends across the Americas are reflected in global, latitudinally-averaged, transects and for other continents. In general, the species richness of taxa such as hummingbirds and amphibians is strongly and positively correlated with precipitation rate and temperature, except in Africa, where high temperatures may limit availability of water.

3.7 Conclusions

In summary, wavelet power spectral analysis provides insight into the coherence between species richness and environmental variables. Species richness is shown to vary as a function of location and scale. Comparisons with topography, temperature and precipitation show that species richness tends to be highly coherent with external forcing at large scales (wavelengths $> 10^4$ km). Phase difference between signals reveals that species richness is in-phase with precipitation and temperature, and anti-phase with elevation and annual temperature range, at these scales. However, these relationships are dependent

on scale and taxon. At smaller scales, richness of bats, songbirds, hummingbirds and amphibians tends to be greatest in the tropics, where calculated coherence highlights the importance of topography and temperature range for determining species richness. Carnivorans, in contrast, show little coherence with environmental variables at these scales in the tropics. Instead, they are most coherent in the vicinity of terrestrial plateaux, for example the Colorado Plateau and Altiplano. These observations suggest that large scale ($> 10^3$ km) variations in environmental variables determine almost all of the distribution of terrestrial vertebrates. Smaller scale ($\lesssim 10^3$ km) variation can play an important role locally, particularly within the tropics. These results highlight the general importance of environmental change at the scale of tens degrees of latitude for determining biodiversity. They also indicate that changes at smaller scales are comparatively more important in the tropics for determining species richness. Crucially, these results could be used to predict the changes in biodiversity that could arise from different future Earth climate change scenarios.

References

Albanese, D., Visintainer, R., Merler, S., Riccadonna, S., Jurman, G., & Furlanello, C., 2012. mlpy: Machine Learning Python.

Allen, A. P., Gillooly, J. F., Savage, V. M., & Brown, J. H., 2006. Kinetic effects of temperature on rates of genetic divergence and speciation, *PNAS*, **103**(24), 9130–9135.

Amante, C. & Eakins, B. W., 2009. ETOPO1 Arc-minute global relief model: Procedures, data sources and analysis, Tech. rep., NOAA, Boulder, Colorado.

Antonelli, A., Kissling, W. D., Flantua, S. G. A., Bermúdez, M. A., Mulch, A., Muellner-Riehl, A. N., Kreft, H., Linder, H. P., Badgley, C., Fjeldså, J., Fritz, S. A., Rahbek, C., Herman, F., Hooghiemstra, H., & Hoorn, C., 2018. Geological and climatic influences on mountain biodiversity, *Nature Geoscience*, **11**, 718–725.

Araújo, M. B. & Rahbek, C., 2006. How Does Climate Change Affect Biodiversity?, *Science*, **313**, 1396–1397.

Archibald, S. B., Bossert, W. H., Greenwood, D. R., & Farrell, B. D., 2010. Seasonality, the latitudinal gradient of diversity, and Eocene insects, *Paleobiology*, **36**(3), 374–398.

Archibald, S. B., Greenwood, D. R., & Mathewes, R. W., 2013. Seasonality, montane beta diversity, and Eocene insects: Testing Janzen's dispersal hypothesis in an equable world, *Palaeogeography, Palaeoclimatology, Palaeoecology*, **371**, 1–8.

549 Balmford, A. & Bond, W., 2005. Trends in the state of nature and their implications for human
550 well-being, *Ecology Letters*, **8**(11), 1218–1234.

551 Barrett, C. B., Travis, A. J., & Dasgupta, P., 2011. On biodiversity conservation and poverty traps,
552 *PNAS*, **108**(34), 13907–13912.

553 Belmaker, J. & Jetz, W., 2011. Cross-scale variation in species richness-environment associations,
554 *Global Ecology and Biogeography*, **20**(3), 464–474.

555 BirdLife International NatureServe, 2011. Bird Species Distribution Maps of the World, BirdLife In-
556 ternational, Cambridge, UK.

557 Buckley, L. B. & Jetz, W., 2007. Environmental and historical constraints on global patterns of am-
558 phibian richness, *Proceedings of the Royal Society B*, **274**, 1167–1173.

559 Buckley, L. B., Hurlbert, A. H., & Jetz, W., 2012. Broad-scale ecological implications of ectothermy
560 and endothermy in changing environments, *Global Ecology and Biogeography*, **21**(9), 873–885.

561 Carl, G., Dormann, C. F., & Kühn, I., 2008. A wavelet-based method to remove spatial autocorrelation
562 in the analysis of species distributional data, *Web Ecology*, pp. 22–29.

563 Carl, G., Doktor, D., Schweiger, O., & Kühn, I., 2016. Assessing relative variable importance across
564 different spatial scales: a two-dimensional wavelet analysis, *Journal of Biogeography*, **43**(12), 2502–
565 2512.

566 Chaudhary, C., Richardson, A. J., Schoeman, D. S., & Costello, M. J., 2021. Global warming is causing
567 a more pronounced dip in marine species richness around the equator, *PNAS*, **118**(15), 1–6.

568 Corenblit, D., Baas, A. C., Bornette, G., Darrozes, J., Delmotte, S., Francis, R. A., Gurnell, A. M., Ju-
569 lien, F., Naiman, R. J., & Steiger, J., 2011. Feedbacks between geomorphology and biota controlling
570 Earth surface processes and landforms: A review of foundation concepts and current understandings,
571 *Earth-Science Reviews*, **106**(3-4), 307–331.

572 Dee, D. P., Uppala, S. M., Simmons, A. J., Berrisford, P., Poli, P., Kobayashi, S., Andrae, U.,
573 Balmaseda, M. A., Balsamo, G., Bauer, P., Bechtold, P., Beljaars, A. C., van de Berg, L., Bidlot,
574 J., Bormann, N., Delsol, C., Dragani, R., Fuentes, M., Geer, A. J., Haimberger, L., Healy, S. B.,
575 Hersbach, H., Hólm, E. V., Isaksen, L., Kållberg, P., Köhler, M., Matricardi, M., Mcnally, A. P.,
576 Monge-Sanz, B. M., Morcrette, J. J., Park, B. K., Peubey, C., de Rosnay, P., Tavolato, C., Thépaut,
577 J. N., & Vitart, F., 2011. The ERA-Interim reanalysis: Configuration and performance of the data
578 assimilation system, *Quarterly Journal of the Royal Meteorological Society*, **137**(656), 553–597.

Dormann, C. F., McPherson, J. M., Araújo, M. B., Bivand, R., Bollinger, J., Carl, G., Davies, R. G., Hirzel, A., Jetz, W., Kissling, W. D., Kühn, I., Ohlemüller, R., Peres-Neto, P. R., Reineking, B., Schröder, B., Schurr, F. M., & Wilson, R., 2007. Methods to account for spatial autocorrelation in the analysis of species distributional data: A review, *Ecography*, **30**(5), 609–628.

Eronen, J. T., Janis, C. M., Chamberlain, C. P., & Mulch, A., 2015. Mountain uplift explains differences in Palaeogene patterns of mammalian evolution and extinction between North America and Europe, *Proceedings of the Royal Society B: Biological Sciences*, **282**(20150136), 1–8.

Fei, S., Phillips, J., & Shouse, M., 2014. Biogeomorphic impacts of invasive species, *Annual Review of Ecology, Evolution, and Systematics*, **45**, 69–87.

Field, R., Hawkins, B. A., Cornell, H. V., Currie, D. J., Diniz-Filho, J. A. F., Guégan, J.-F., Kaufman, D. M., Kerr, J. T., Mittelbach, G. G., Oberdorff, T., O'Brien, E. M., & Turner, J. R. G., 2009. Spatial species-richness gradients across scales: A meta-analysis, *Journal of Biogeography*, **36**(1), 132–147.

Fritz, S. A., Eronen, J. T., Schnitzler, J., Hof, C., Janis, C. M., Mulch, A., Böhning-Gaese, K., & Graham, C. H., 2016. Twenty-million-year relationship between mammalian diversity and primary productivity, *PNAS*, **113**(39), 10908–10913.

Gaston, K. J., 2000. Global patterns in biodiversity, *Nature*, **405**(6783), 220–227.

Ghalambor, C. K., Huey, R. B., Martin, P. R., Tewksbury, J. J., & Wang, G., 2006. Are mountain passes higher in the tropics? Janzen's hypothesis revisited, *Integrative and Comparative Biology*, **46**(1), 5–17.

Gillman, L. N., Wright, S. D., Cusens, J., McBride, P. D., Malhi, Y., & Whittaker, R. J., 2015. Latitude, productivity and species richness, *Global Ecology and Biogeography*, **24**(1), 107–117.

Goddard Earth Sciences Data and Information Services Center, 2017. TRMM (TMPA/3B43) Rainfall Estimate L3 1 Month 0.25 Degree x 0.25 Degree V7.

Grinsted, A., Moore, J. C., & Jevrejeva, S., 2004. Application of the cross wavelet transform and wavelet coherence to geophysical time series, *Nonlinear Processes in Geophysics*, **11**(5/6), 561–566.

Hagen, O., Skeels, A., Onstein, R. E., Jetz, W., & Pellissier, L., 2021. Earth history events shaped the evolution of biodiversity across tropical rainforests, *PNAS*, **118**(40), 1–11.

Hampe, A. & Petit, R. J., 2005. Conserving biodiversity under climate change: The rear edge matters, *Ecology Letters*, **8**(5), 461–467.

Hawkins, B. A., Porter, E. E., & Diniz-Filho, J. A. F., 2003. Productivity and history as predictors of the latitudinal diversity gradient of terrestrial birds, *Ecology*, **84**(6), 1608–1623.

Hijmans, R. J., Cameron, S. E., Parra, J. L., Jones, P. G., & Jarvis, A., 2005. Very high resolution interpolated climate surfaces for global land areas, *International Journal of Climatology*, **25**(15), 1965–1978.

Hillebrand, H., 2004. On the generality of the latitudinal diversity gradient, *American Naturalist*, **163**(2), 192–211.

Hurlbert, A. H. & Jetz, W., 2007. Species richness, hotspots, and the scale dependence of range maps in ecology and conservation, *PNAS*, **104**(33), 13384–13389.

International Union for Conservation of Nature, 2021. The IUCN Red List of Threatened Species.

Janzen, D. H., 1967. Why Mountain Passes are Higher in the Tropics, *The American Naturalist*, **101**(919), 233–249.

Jarvis, A., Reuter, H. I., Nelson, A., & Guevara, E., 2008. Hole-filled seamless SRTM data V4.

Jenkins, C. N. & Joppa, L., 2009. Expansion of the global terrestrial protected area system, *Biological Conservation*, **142**(10), 2166–2174.

Jenkins, C. N., Pimm, S. L., & Joppa, L. N., 2013. Global patterns of terrestrial vertebrate diversity and conservation, *PNAS*, **110**(28), E2603–E2610.

Jenkins, J., Stephenson, S. N., Martínez-Garzón, P., Bohnhoff, M., & Nurlu, M., 2020. Crustal Thickness Variation Across the Sea of Marmara Region, NW Turkey: A Reflection of Modern and Ancient Tectonic Processes, *Tectonics*, **39**(7), 1–18.

Jones, L. A., Mannion, P. D., Farnsworth, A., Bragg, F., & Lunt, D. J., 2022. Climatic and tectonic drivers shaped the tropical distribution of coral reefs, *Nature Communications*, **13**(3120), 1–10.

Karger, D. N., Conrad, O., Böhner, J., Kawohl, T., Kreft, H., Soria-Auza, R. W., Zimmermann, N. E., Linder, H. P., & Kessler, M., 2017. Climatologies at high resolution for the earth's land surface areas, *Scientific Data*, **4**(170122), 1–20.

Kass, J. M., Guénard, B., Dudley, K. L., Jenkins, C. N., Azuma, F., Fisher, B. L., Parr, C. L., Gibb, H., Longino, J. T., Ward, P. S., Chao, A., Lubertazzi, D., Weiser, M., Jetz, W., Guralnick, R., Blatrix, R., Des Lauriers, J., Donoso, D. A., Georgiadis, C., Gomez, K., Hawkes, P. G., Johnson, R. A., Lattke, J. E., MacGown, J. A., Mackay, W., Robson, S., Sanders, N. J., Dunn, R. R., & Economo, E. P., 2022. The global distribution of known and undiscovered ant biodiversity, *Science Advances*, **9908**, 1–16.

Keil, P. & Chase, J. M., 2019. Global patterns and drivers of tree diversity integrated across a continuum of spatial grains, *Nature Ecology and Evolution*, **3**(3), 390–399.

Keitt, T. H., 2007. On the quantification of local variation in biodiversity scaling using wavelets, in *Scaling Biodiversity*, edited by D. Storch, P. Marquet, & J. Brown, chap. 9, pp. 168–180, Cambridge University Press.

Kessler, M., Salazar, L., Homeier, J., & Kluge, J., 2014. Species richness-productivity relationships of tropical terrestrial ferns at regional and local scales, *Journal of Ecology*, **102**(6), 1623–1633.

Krieger, S., Freij, N., Brazhe, A., Torrence, C., & Compo, G. P., 2020. *PyCWT: A Python module for continuous wavelet spectral analysis*.

Lawrimore, J. H., Menne, M. J., Gleason, B. E., Williams, C. N., Wuertz, D. B., Vose, R. S., & Rennie, J., 2011. An overview of the Global Historical Climatology Network monthly mean temperature data set, version 3, *Journal of Geophysical Research Atmospheres*, **116**(19), 1–18.

Liu, Y., Liang, X. S., & Weisberg, R. H., 2007. Rectification of the bias in the wavelet power spectrum, *Journal of Atmospheric and Oceanic Technology*, **24**(12), 2093–2102.

Ma, Z. & Zhang, L., 2015. Modeling bird species richness at multiple spatial scales using two-dimensional wavelet analysis, *Forest Science*, **61**(1), 1–16.

Mannion, P. D., Upchurch, P., Benson, R. B. J., & Goswami, A., 2014. The latitudinal biodiversity gradient through deep time, *Trends in Ecology and Evolution*, **29**(1), 42–50.

Marsh, C. J., Sica, Y. V., Burgin, C. J., Dorman, W. A., Anderson, R. C., del Toro Mijares, I., Vigneron, J. G., Barve, V., Dombrowik, V. L., Duong, M., Guralnick, R., Hart, J. A., Maypole, J. K., McCall, K., Ranipeta, A., Schuerkmann, A., Torselli, M. A., Lacher, T., Mittermeier, R. A., Rylands, A. B., Sechrest, W., Wilson, D. E., Abba, A. M., Aguirre, L. F., Arroyo-Cabrales, J., Astúa, D., Baker, A. M., Braulik, G., Braun, J. K., Brito, J., Busher, P. E., Burneo, S. F., Camacho, M. A., Cavallini, P., de Almeida Chiquito, E., Cook, J. A., Cserkész, T., Csorba, G., Cuéllar Soto, E., da Cunha Tavares, V., Davenport, T. R. B., Deméré, T., Denys, C., Dickman, C. R., Eldridge, M. D. B., Fernandez-Duque, E., Francis, C. M., Frankham, G., Franklin, W. L., Freitas, T., Friend, J. A., Gadsby, E. L., Garbino, G. S. T., Gaubert, P., Giannini, N., Giarla, T., Gilchrist, J. S., Gongora, J., Goodman, S. M., Gursky-Doyen, S., Hackländer, K., Hafner, M. S., Hawkins, M., Helgen, K. M., Heritage, S., Hinckley, A., Hintsche, S., Holden, M., Holekamp, K. E., Honeycutt, R. L., Huffman, B. A., Humle, T., Hutterer, R., Ibáñez Ulargui, C., Jackson, S. M., Janecka, J., Janecka, M., Jenkins, P., Juškaitis, R., Juste, J., Kays, R., Kilpatrick, C. W., Kingston, T., Koprowski, J. L., Kryštufek, B., Lavery, T., Lee, T. E., Leite, Y. L. R., Novaes, R. L. M., Lim,

672 B. K., Lissovsky, A., López-Antoñanzas, R., López-Baucells, A., MacLeod, C. D., Maisels, F. G.,
673 Mares, M. A., Marsh, H., Mattioli, S., Meijaard, E., Monadjem, A., Morton, F. B., Musser, G.,
674 Nadler, T., Norris, R. W., Ojeda, A., Ordóñez-Garza, N., Pardiñas, U. F. J., Patterson, B. D.,
675 Pavan, A., Pennay, M., Pereira, C., Prado, J., Queiroz, H. L., Richardson, M., Riley, E. P., Rossiter,
676 S. J., Rubenstein, D. I., Ruelas, D., Salazar-Bravo, J., Schai-Braun, S., Schank, C. J., Schwitzer,
677 C., Sheeran, L. K., Shekelle, M., Shenbrot, G., Soisook, P., Solari, S., Southgate, R., Superina, M.,
678 Taber, A. B., Talebi, M., Taylor, P., Thong, V. D., Ting, N., Tirira, D. G., Tsang, S., Turvey, S. T.,
679 Valdez, R., Van Cakenberghe, V., Veron, G., Wallis, J., Wells, R., Whittaker, D., Williamson, E. A.,
680 Wittemyer, G., Woinarski, J., Zinner, D., Upham, N. S., & Jetz, W., 2022. Expert range maps of
681 global mammal distributions harmonised to three taxonomic authorities, *Journal of Biogeography*,
682 **49**(5), 979–992.

683 Mori, A. S., Sasaki, T., Kagami, M., Miki, T., & Yasuhara, M., 2022. Feedbacks Between Biodiversity
684 and Climate Change, in *The Ecological and Societal Consequences of Biodiversity Loss*, chap. 13,
685 pp. 281–304, Princeton University Press.

686 Nogués-Bravo, D., Rodríguez-Sánchez, F., Orsini, L., de Boer, E., Jansson, R., Morlon, H., Fordham,
687 D. A., & Jackson, S. T., 2018. Cracking the Code of Biodiversity Responses to Past Climate Change,
688 *Trends in Ecology and Evolution*, **33**(10), 765–776.

689 Norris, R. D., Kirtland Turner, S., Hull, P. M., & Ridgwell, A., 2013. Marine ecosystem responses to
690 Cenozoic global change, *Science*, **341**(6145), 492–498.

691 Palmer, M. W. & White, P. S., 1994. Scale Dependence and the Species-Area Relationship, *The*
692 *American Naturalist*, **144**(5), 717–740.

693 Polato, N. R., Gill, B. A., Shah, A. A., Gray, M. M., Casner, K. L., Barthelet, A., Messer, P. W.,
694 Simmons, M. P., Guayasamin, J. M., Encalada, A. C., Kondratieff, B. C., Flecker, A. S., Thomas,
695 S. A., Ghalambor, C. K., Poff, N. L., Funk, W. C., & Zamudio, K. R., 2018. Narrow thermal tolerance
696 and low dispersal drive higher speciation in tropical mountains, *PNAS*, **115**(49), 12471–12476.

697 Rahbek, C. & Graves, G. R., 2001. Multiscale assessment of patterns of avian species richness, *PNAS*,
698 **98**(8), 4534–4539.

699 Rahbek, C., Borregaard, M. K., Colwell, R. K., Dalsgaard, B., Holt, B. G., Morueta-Holme, N.,
700 Nogues-Bravo, D., Whittaker, R. J., & Fjeldså, J., 2019. Humboldt's enigma: What causes global
701 patterns of mountain biodiversity?, *Science*, **365**(6458), 1108–1113.

702 Roberts, G. G. & Mannion, P. D., 2019. Timing and periodicity of Phanerozoic marine biodiversity
703 and environmental change, *Scientific Reports*, **9**(1), 6116.

Roberts, G. G., White, N., & Lodhia, B. H., 2019. The Generation and Scaling of Longitudinal River Profiles, *Journal of Geophysical Research: Earth Surface*, **124**, 17.

Rolland, J., Condamine, F. L., Beeravolu, C. R., Jiguet, F., & Morlon, H., 2015. Dispersal is a major driver of the latitudinal diversity gradient of Carnivora, *Global Ecology and Biogeography*, **24**(9), 1059–1071.

Rolland, J., Silvestro, D., Schluter, D., Guisan, A., Broennimann, O., & Salamin, N., 2018. The impact of endothermy on the climatic niche evolution and the distribution of vertebrate diversity, *Nature Ecology and Evolution*, **2**(3), 459–464.

Saupe, E. E., 2021. Explanations for tropical diversity gradients are rooted in the deep past, *PNAS*, **118**(43), 1–3.

Schneider, U., Becker, A., Finger, P., Meyer-Christoffer, A., Ziese, M., & Rudolf, B., 2014. GPCC's new land surface precipitation climatology based on quality-controlled in situ data and its role in quantifying the global water cycle, *Theoretical and Applied Climatology*, **115**(1-2), 15–40.

Skeels, A., Bach, W., Hagen, O., Jetz, W., & Pellissier, L., 2022. Temperature-Dependent Evolutionary Speed Shapes the Evolution of Biodiversity Patterns Across Tetrapod Radiations, *Systematic Biology*, pp. 1–16.

Song, H., Huang, S., Jia, E., Dai, X., Wignall, P. B., & Dunhill, A. M., 2020. Flat latitudinal diversity gradient caused by the Permian-Triassic mass extinction, *Proceedings of the National Academy of Sciences of the United States of America*, **117**(30), 17578–17583.

Storch, D., Marquet, P., & Brown, J., 2007. *Scaling Biodiversity*, Cambridge University Press.

Torrence, C. & Compo, G. P., 1998. A practical guide to wavelet analysis, *Bulletin of the American Meteorological Society*, **79**(1), 61–78.

Wapenhans, I., Fernandes, V. M., O'Malley, C., White, N., & Roberts, G. G., 2021. Scale-Dependent Contributors to River Profile Geometry, *Journal of Geophysical Research: Earth Surface*, **126**, 1–25.

Wessel, P., Luis, J., Uieda, L., Scharroo, R., Wobbe, F., Smith, W. H. F., & Tian, D., 2019. The Generic Mapping Tools Version 6, *Geochemistry, Geophysics, Geosystems*, **20**, 1–9.

Willig, M. R., Kaufman, D. M., & Stevens, R. D., 2003. Latitudinal Gradients of Biodiversity: Pattern, Process, Scale, and Synthesis, *Annual Review of Ecology, Evolution, and Systematics*, **34**, 273–309.

Yasuhara, M. & Deutsch, C. A., 2022. Paleobiology provides glimpses of future ocean, *Science*, **375**(6576), 25–26.

734 Yasuhara, M., Iwatani, H., Hunt, G., Okahashi, H., Kase, T., Hayashi, H., Irizuki, T., Aguilar, Y. M.,
735 Fernando, A. G. S., & Renema, W., 2017. Cenozoic dynamics of shallow-marine biodiversity in the
736 Western Pacific, *Journal of Biogeography*, **44**(3), 567–578.

737 Yasuhara, M., Huang, H.-H. M., Hull, P., Rillo, M. C., Condamine, F. L., Tittensor, D. P., Kučera,
738 M., Costello, M. J., Finnegan, S., O'Dea, A., Hong, Y., Bonebrake, T. C., McKenzie, N. R., Doi, H.,
739 Wei, C.-L., Kubota, Y., & Saupe, E. E., 2020. Time Machine Biology: Cross-Timescale Integration
740 of Ecology, Evolution, and Oceanography, *Oceanography*, **33**(2), 17–28.

741 Yasuhara, M., Wei, C.-L., Kucera, M., Costello, M. J., Tittensor, D. P., Kiessling, W., Bonebrake,
742 T. C., Tabor, C. R., Feng, R., Baselga, A., Kretschmer, K., Kusumoto, B., & Kubota, Y., 2020.
743 Past and future decline of tropical pelagic biodiversity, *PNAS*, **117**(23), 12891–12896.

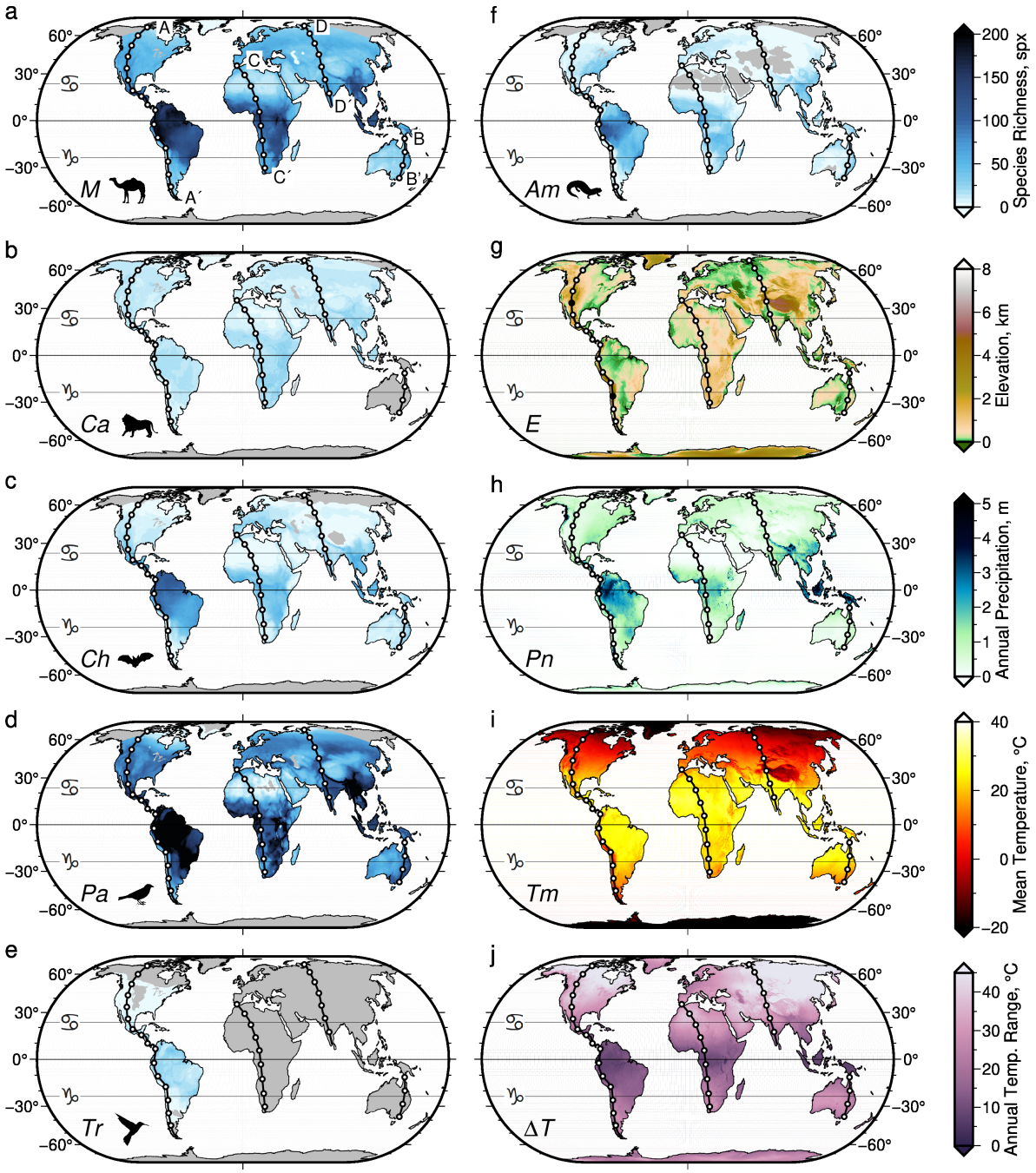

Figure 1: Global patterns of species richness and environment. (a) All Mammalia (*M*, mammals), (b) Carnivora (*Ca*, carnivorans), (c) Chiroptera (*Ch*, bats), (d) Passeriformes (*Pa*, songbirds), (e) Trochilidae (*Tr*, hummingbirds), (f) Amphibia (*Am*, amphibians); spx = species per 10×10 km pixel (Jenkins *et al.*, 2013); horizontal lines = Tropics of Cancer (northern), Capricorn (southern), and Equator; A—A′ = transect through Americas investigated here; B—B′, C—C′, D–D′ = transects investigated in Supporting Information. Global latitudinal mean transects also studied therein and in Figure 4. (g) Elevation (*E*) from ETOPO1 global model with horizontal resolution of 1 arc-minute (Amante & Eakins, 2009); filled circles on A—A′ = Colorado Plateau/Mexican Highlands and Andean Altiplano. (h)–(j) Mean annual precipitation rate (*Pn*), temperature (*Tm*), and temperature range (ΔT) from 1981–2010 (Karger *et al.*, 2017).

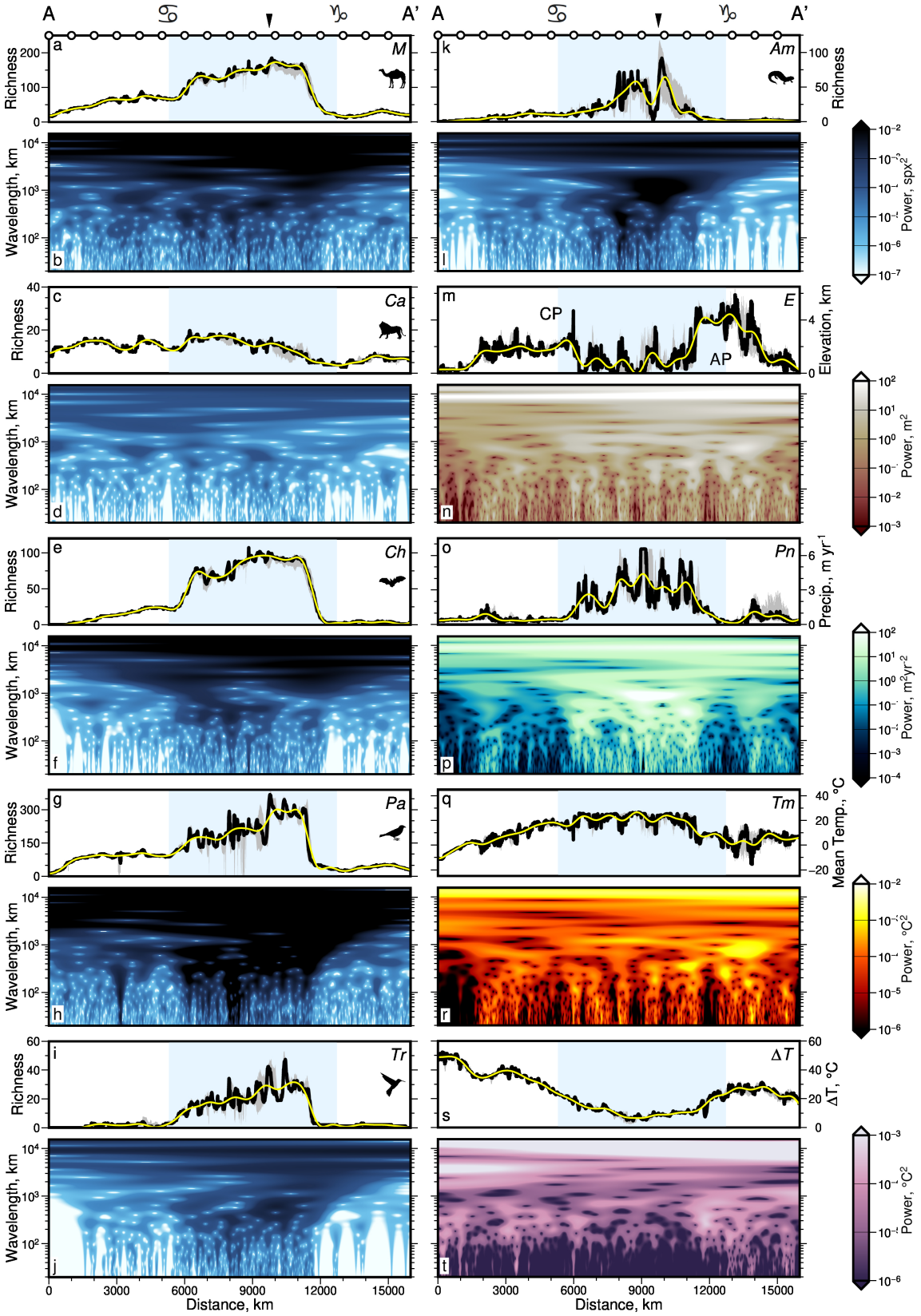

Figure 2

Figure 2 ***(preceding page)*****: Wavelet transforms of species richness and environment**. (a) Black line = species richness of Mammalia (M) along transect A—A′; gray bands = 100 km wide swaths centred on A—A′; blue bands = tropical latitudes; white circles are shown every 1000 km, see transect A—A′ in Figure 1; black arrow and symbols above top axis = Equator and tropics as in Figure 1. Yellow line = inverse wavelet transform of signal, filtering to pass only wavelengths > 1000 km; mean difference to input signal = 3.0 ± 3.3 (1σ) spx. (b) Continuous wavelet transform of mammal richness spatial series (black line in panel a). Colors = rectified spectral power as a function of location and scale (wavelength); spx = species per pixel. (c)–(t) As (a)–(b) but for Carnivora (Ca), Chiroptera (Ch), Passeriformes (Pa), Trochilidae (Tr), Amphibia (Am), elevation (E), mean annual precipitation rate (Pn), temperature (Tm) and temperature range (ΔT) along transect A—A′ (Amante & Eakins, 2009; Jenkins *et al.*, 2013; Karger *et al.*, 2017). Mean differences between signals and inverse transforms filtered to remove wavelengths < 1000 km = 0.7 ± 0.6 spx (Ca), 1.5 ± 2.1 spx (Ch), 11.6 ± 16.7 spx (Pa), 1.5 ± 2.5 spx (Tr), 2.9 ± 5.3 spx (Am), 0.36 ± 0.3 km (E), 0.35 $^{+0.5}_{-0.35}$ m/yr (Pn), 2.2 ± 2.2 °C (Tm), and 1.2 ± 1.1 °C (ΔT). See Supporting Information for results for transects B—B′, C—C′, D—D′ and average global latitudinal transect. Note high spectral power concentrated at wavelengths > 10^3 km for all series. High species richness power (darker patches) at shorter wavelengths tends to be concentrated within the tropics.

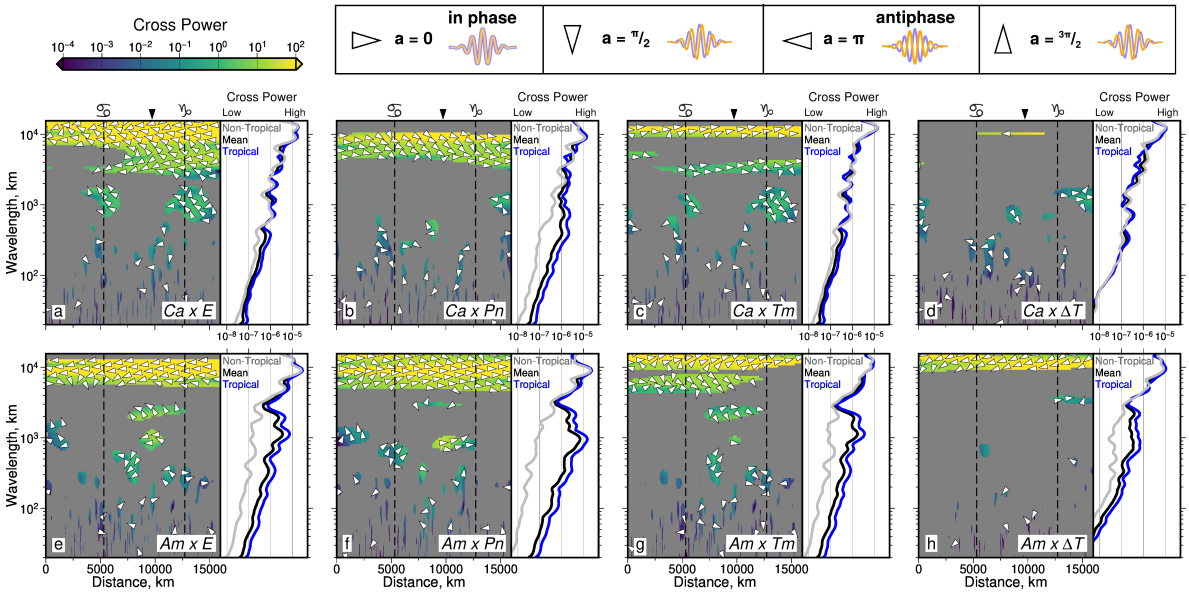

Figure 3: Coherence, cross power, and phase difference between species richness and environmental variables. (a) Comparison of Carnivora (Ca) and elevation (E) as a function of location and scale along transect A—A′ (Figures 1–2). Colors = cross wavelet power; yellow = co-located large (positive or negative) amplitude signals. Gray masks regions with coherence below 90% significance level (see body text, Materials and Methods). Arrows = phase difference between spatial series: right/left pointing = in-phase/anti-phase (see guide above panels b–d). Black arrow and symbols above plot = Equator and tropics, as in Figure 1. Side panel: black/blue/gray lines = distance-averaged cross wavelet power of all/tropical/non-tropical latitudes (see Figure 2). High cross power = large co-located amplitudes in the two spatial series. (b)–(d) Comparison of Carnivora and mean annual precipitation rate (Pn), temperature (Tm) and annual temperature range (ΔT). (e)–(h) Comparison of amphibian species richness and same environmental variables as panels a–d. Statistically significant coherence is concentrated at wavelengths > 10^3 km, where species tend to be in- or anti-phase with environmental variables. The least statistically significant coherence is for Carnivora and temperature range (note gray mask across most of panel d).

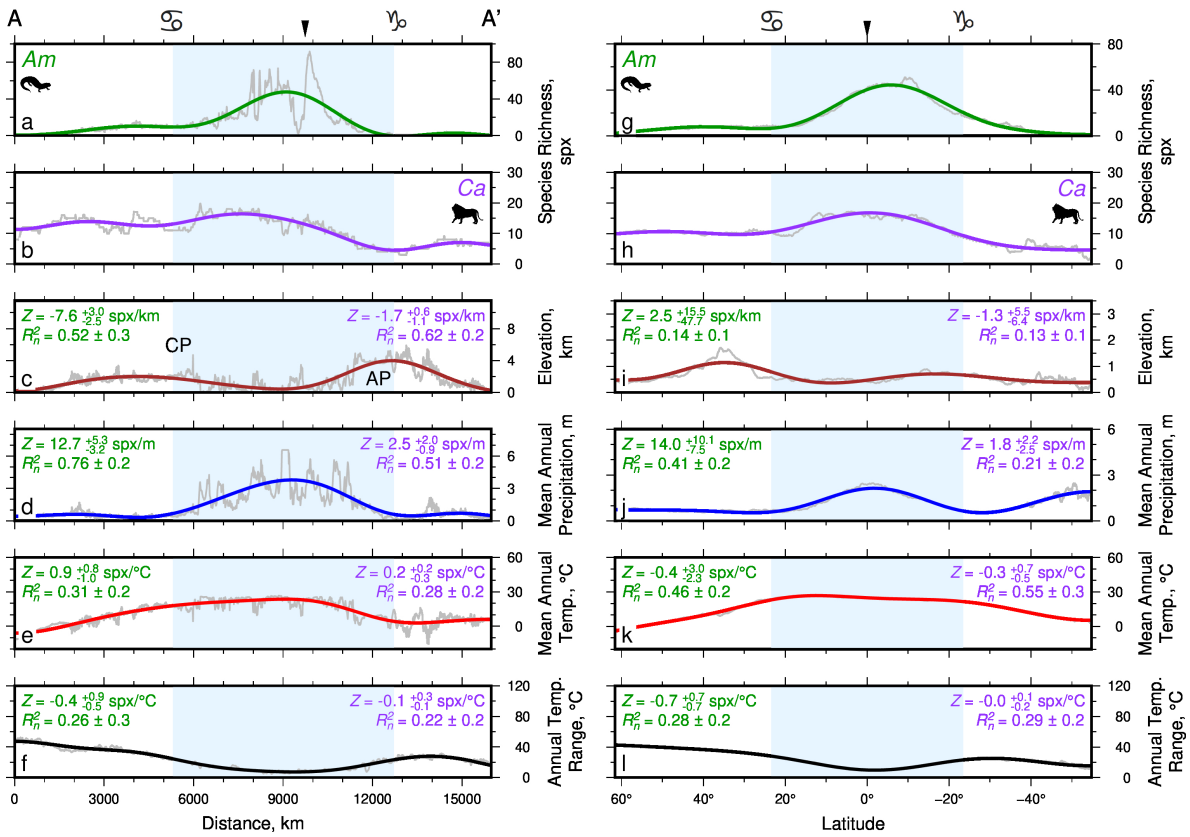

Figure 4: Summary of coherence between species richness and environmental variables at large scales. (a-f) Species richness and environmental variables along Americas transect A—A′ (see Figures 1–2). Blue band = tropical latitudes; black arrow = Equator; symbols above x axis = Tropics of Cancer and Capricorn. (a) Amphibian species richness. Gray = full-resolution observed species richness trend (see Figure 2k). Green = inverse wavelet transform showing filtered amphibian species richness at wavelengths $\geq$ 3756 km (i.e. one quarter of transect length scale). Mean difference between gray and green lines = 4.4 spx. (b) As (a) but for carnivoran species richness. Mean difference between gray and green lines = 1.2 spx. (c)–(f) As (a)–(b) but for elevation, mean annual precipitation, mean temperature, and annual temperature range, respectively. Z, R_n^2 = mean admittance and coherence, respectively, between species richness and given environmental variable. Green text = admittance for amphibian species richness; purple text = admittance for carnivoran species richness. (g)–(l) As (a)–(f) but for mean global latitudinal transects.